

# BrightView XCT – flat-panel cone-beam CT with iterative reconstruction for localization and attenuation correction

E. Hansis, PhD, A. Da Silva, PhD, H. Hines, PhD, J. Garrard, D. Sowards-Emmerd, PhD, and L. Shao, PhD  
Philips Healthcare – Nuclear Medicine, San Jose, CA

The BrightView XCT (Philips Healthcare, Cleveland, OH) is a unique SPECT/CT device, in which CT imaging functionality is provided by a flat-panel based cone-beam CT component. We summarize the current methods for X-ray data processing and reconstruction, including iterative reconstruction. System performance measurements and example clinical cases are shown.

## Materials and methods

### BrightView XCT scanner

The BrightView XCT is a hybrid medical imaging system integrating a fully-featured variable angle nuclear medicine gamma camera with a flat-panel cone-beam CT (CBCT) component used for localization and attenuation correction of the SPECT data.[1] A novel aspect of this system is its unique design; the flat-panel CBCT component is mounted on the same rotatable gantry as the SPECT component. This setup reduces room size requirements and system weight compared to using a separate CT gantry. Furthermore, it enables co-planar SPECT and CBCT imaging and high-resolution isotropic CT reconstruction.

The CBCT component consists of an X-ray source and a flat-panel X-ray detector (Figure 1). The detector, measuring 40 cm × 30 cm, is mounted at a lateral offset with respect to the X-ray source. This way, a single X-ray projection covers slightly more than half of the CT field of view (FoV). With a 360° rotation of the gantry, a 47 cm diameter transverse FoV and a 14.4 cm axial length along the patient can be imaged. Larger axial

extents are imaged in a step-and-shoot fashion, by combining volumes from several XCT spins.

The flat-panel based system enables reconstruction with a 1 mm isotropic voxel size for the entire FoV and as small as 0.33 mm isotropic voxel size for high-resolution sub-volume reconstructions.

Either 300 or 720 X-ray projections are acquired for each spin during 12, 24, or 60 second rotation time (depending on the protocol). These rotation speeds allow for flexible breathing protocols: the XCT scan can be performed either during breath holding or during shallow tidal respiration depending on the clinical application. Since respiratory motion and peristalsis cause the structures in the chest, abdomen and pelvis to change position and shape, the best image quality for localization studies of the chest, abdomen and pelvis will be achieved during breath holding using the 12 second rotation. Shallow tidal breathing is usually adequate for extremity and head studies, using either the 12 or 24 second rotation, since these areas are generally not affected by respiratory motion.

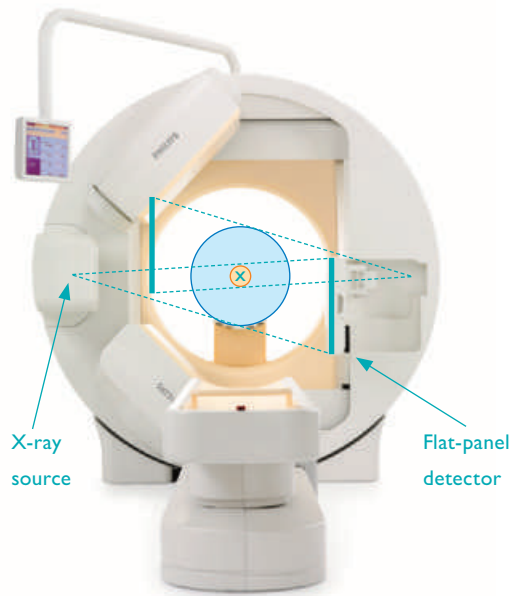


**Figure 1** BrightView XCT system with sketch of CBCT geometry. The X-ray acquisition cone (dashed lines) is shown for two opposite gantry rotation angles. The blue disk indicates the transaxial FoV, the small orange disk a central overlap region.

For attenuation correction scans in myocardial perfusion studies, shallow tidal breathing with the 60 second rotation is preferred in order to average the attenuation data over multiple respiratory cycles to match the position of the heart during the SPECT study.

The CBCT component differs from a conventional CT in terms of detector type, acquisition geometry, and axial FoV size. Therefore, three-dimensional (3D) reconstruction of the CBCT data requires special methods. Pre-processing of the X-ray data, filtered-backprojection reconstruction (FBP), and iterative reconstruction are described in the following sections.<sup>1</sup> System performance data from phantom measurements are presented, as well as example patient cases.

<sup>1</sup> The described features are available on BrightView XCT systems with software version 2.5 or later.

### Pre- and post-processing

The X-ray projection data of an XCT acquisition must be pre-processed prior to reconstruction, to calibrate system characteristics and to compensate for various physical effects:

- 1. Detector corrections:** Detector offset, uniformity, and gain are corrected using dark detector frames and air scans as reference. Defective detector pixels are masked.
- 2. Incident intensity ( $I_0$ ) calibration:** The measured projection values are normalized to the incident X-ray intensity as determined from calibration air scans.
- 3. Adaptive filter:** Projection regions with counts below a defined threshold are filtered to reduce streak artifacts in the reconstruction. Higher-count regions remain unchanged, to retain detail and sharpness.[2]
- 4. De-blurring corrections:** The data are corrected for blurring effects that occur close to the X-ray source and in the detector.
- 5. Scatter correction:** Scattered radiation in the X-ray projections is subtracted using an object-dependent scatter estimation and correction method.[3]
- 6. Beam hardening correction:** An object-dependent beam-hardening correction compensates for spectral characteristics of the source spectrum and of the absorption in the scanned object.[3]
- 7. Low-pass filtration:** A smoothing filter is applied to the data to reduce noise. Two default filter values are provided, one optimized for soft tissue imaging and the other for bone imaging. However, the filter sharpness can be adjusted by the user to achieve an optimum trade-off between noise reduction and sharpness for a given application.

The system geometry for each projection, i.e., the precise positions of X-ray source and detector, are determined by calibration scans and are used in the 3D reconstruction. After reconstruction, ring artifacts are removed from the volume image in a post-processing step. Finally, the intensity of the volume image is calibrated to improve the accuracy of reported Hounsfield Unit (HU) values.

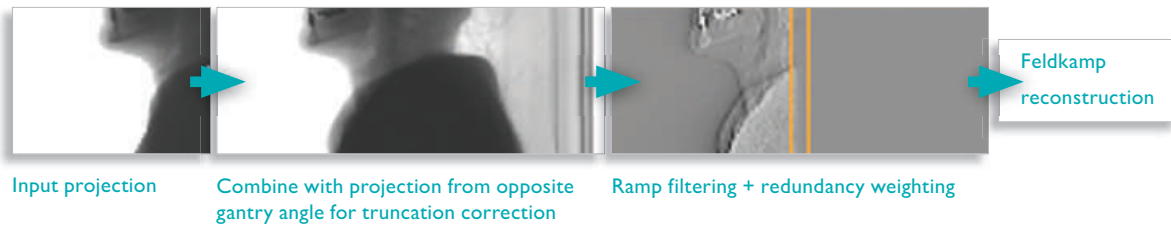


**Figure 2** Outline of the unique steps required for the FBP reconstruction method.

### Filtered-backprojection reconstruction

Almost all current CT scanners employ a filtered-backprojection method (FBP) for reconstruction. For the BrightView XCT, with its offset-detector acquisition geometry, a special FBP method is used,[4] which is a variant of the widely used Feldkamp reconstruction method.[5]

Figure 2 shows the steps involved in the FBP reconstruction. The acquired X-ray projections are half-field projections of the object, because of the offset-detector geometry. The resulting truncation in the object center is compensated by combining each projection with one from the respective opposite gantry angle. On the combined projection, ramp filtering is performed. Additionally, a weighting function is applied to handle the central overlap region (small orange disk in Figure 1). The projection extension is discarded by the weighting. The thus prepared projections are back-projected with the Feldkamp method to generate the volume image.

FBP reconstruction provides a quick volume image for a first review of the acquired data. It can also be used for high-resolution sub-volume reconstruction

of a region of interest. However, the method relies on certain mathematical assumptions relating to the cone-beam geometry and the truncation compensation at the center of the field of view. These hold only approximately for the XCT acquisition geometry. Deviations can cause artifacts in FBP reconstructions, such as left-right intensity imbalance or HU jumps across borders between consecutive XCT segments. Such problems are mitigated by iterative reconstruction.

### Iterative reconstruction

The basic principle of iterative reconstruction is outlined in Figure 3. The process starts with an initial estimate of the volume image  $f$ . This estimated volume is forward-projected for each gantry angle, resulting in estimated projections  $y'$ . The forward projection can be expressed mathematically as a matrix multiplication  $y' = Af$ , where  $A$  is a projection matrix. The estimated projections are compared to the measured projection data  $y$ , and error projections  $c$  are computed from the difference. In a third step, the volume image estimate is updated by back-projecting the error projections across the volume, to update the volume image estimate  $f \rightarrow f + A^T c$ . Here,  $A^T$  signifies the matrix transpose of  $A$ . The whole process is repeated in an iterative fashion, refining the volume image.

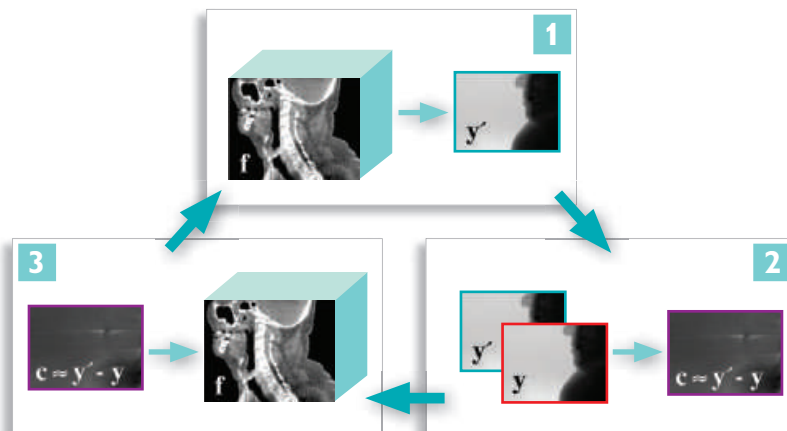


**Figure 3** Outline of iterative reconstruction steps:  
**1** calculating estimated X-ray projections by forward projecting the current volume image estimate;  
**2** computing error projections;  
**3** applying corrections to the volume image.  
 These steps are repeated in an iterative fashion, refining the volume image. Symbols are described in the text.

There exist many variants of iterative reconstruction methods, differing mainly in how correction projections are computed and applied to the volume. For XCT reconstruction, an iterative method called SART [6] is used to create an initial image estimate, followed by several iterations of an ordered-subset maximum-likelihood method.[7] These methods had to be modified for the special XCT acquisition conditions; details can be found in Ref. [8].

The advantage of using iterative reconstruction over FBP is that it can handle the native truncated projections and that the forward projection step can accurately model the cone-beam geometry. Additionally, the maximum-likelihood method includes a model of the acquisition noise, which can lead to reduced noise in the reconstruction. Iterative reconstruction is challenging to implement in a clinical setting because it is very computationally intensive. As mitigation, the XCT iterative reconstruction computation was implemented on a graphics processing

unit (GPU), resulting in reconstruction times of less than 5 minutes per XCT segment (for 1 mm isotropic voxels, 144 slices). Furthermore, in most clinical workflows the XCT scan is performed before the SPECT acquisition. When this is done, the iterative reconstruction can be computed in the background during the SPECT acquisition, with all datasets being ready for review at the end of the study.

## Results and discussion

### System performance

In the following, typical XCT system performance measurements are presented. Figure 4 (left) shows the water uniformity layer of the BrightView XCT Quality Assurance phantom. Noise, spatial uniformity, and water value accuracy can be read from the indicated measurements. The insert layer of the phantom, containing inserts of various materials, is shown in Figure 4 (below). Measured and expected HU values are summarized in Table 1.

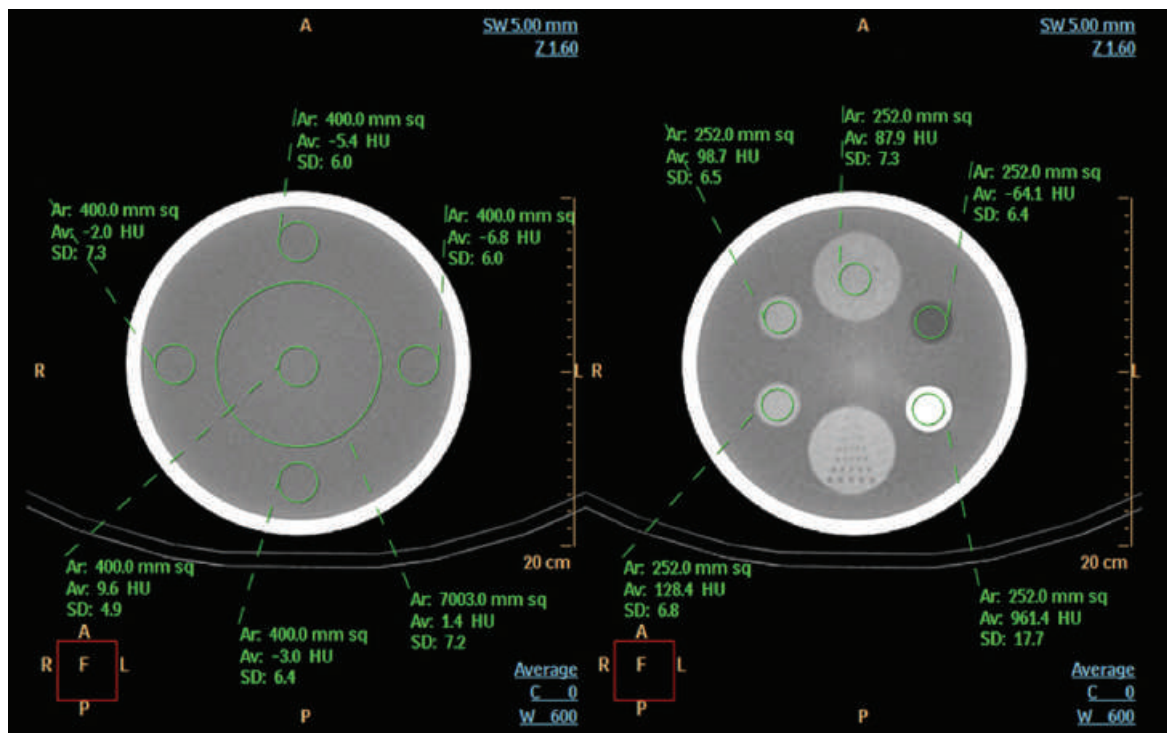


**Figure 4** XCT system performance measurements on a QA phantom. (Left) Uniformity water layer with noise and uniformity measurements. (Right) Insert layer with measurements of inserts of various materials. Reconstructions were generated with 1 mm voxel size and are shown with 5 mm slice thickness. Indicated for each region of interest (ROI) are the measurement area (Ar), average value (Av), and standard deviation (SD).

**Table 1 Measured HU values from Figure 4 and expected values**

Measured area	Measured value (HU)	Expected value (HU)
Water, large Rol	-3.0	0 ± 40
Water, minimum of small Rols	-6.8	0 ± 40
Water, maximum of small Rols	9.6	0 ± 40
Polyethylene insert	-64.1	-70 ± 40
Teflon insert	961.4	950 ± 75
Acrylic insert	128.4	140 ± 40
Lexan insert	98.7	116 ± 40
Nylon insert	87.9	100 ± 40

It should be noted that the HU specification range for the various materials is not as stringent as with conventional CT scanners. The BrightView XCT system was designed as a device where the XCT images are used for localization and attenuation correction of the SPECT images. As such, a ±40 HU maximum range in the value of water and other low density materials and ±75 HU for Teflon do not hinder the display of images for localization tasks, where default window widths of 360 HU (narrowest window – abdomen default window) and 2000 HU (widest window – bone default window) are used. For attenuation correction, the software that converts the XCT image from HU values to linear

attenuation coefficients first segments the XCT image so that values between -150 HU and +150 HU are treated as water. Therefore, variations of up to ±40 HU in the HU value for water and other low density materials would not adversely affect the attenuation correction.

The high-resolution imaging capabilities of the BrightView XCT are demonstrated in Figure 5 on the line-pair gauge of a Catphan® high resolution module (CTP528, The Phantom Laboratory, Greenwich NY, USA). This reconstruction was performed on a 0.33 mm voxel grid using FBP.<sup>2</sup> A maximum of 15 lp/cm can be resolved.

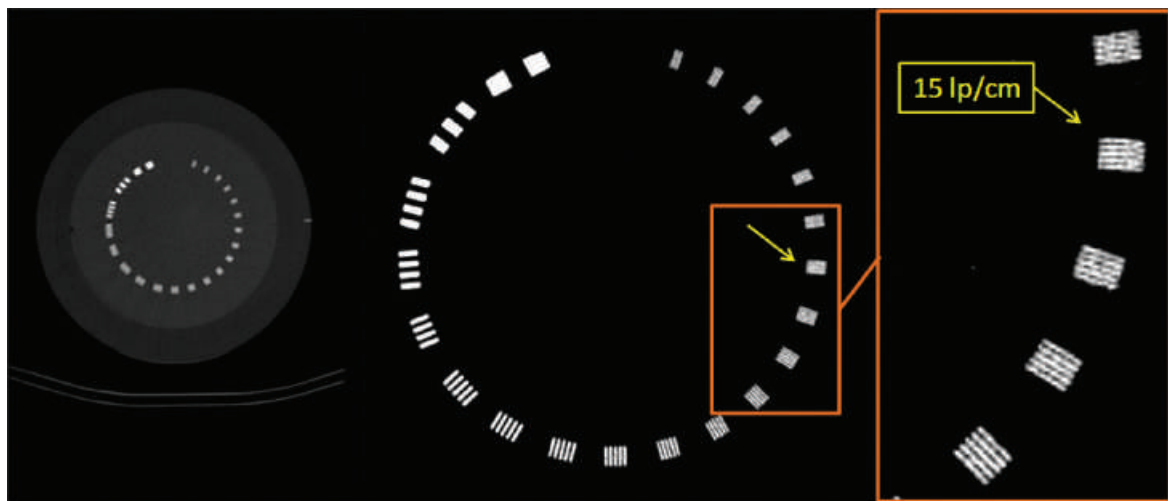


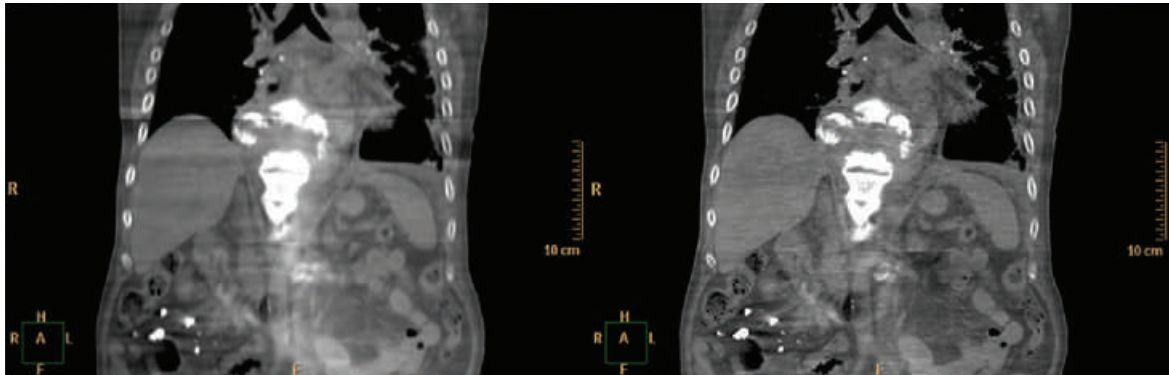
**Figure 5** Catphan® CTP528 high-resolution module. (Left) Overview of module (Level/Window 900/2000 HU). (Middle) Zoomed high-resolution reconstruction of inserts with 0.33 mm voxel size (Level/Window 1000/1000 HU). (Right) Close-up view of inserts. Up to 15 lp/cm can be resolved.

<sup>2</sup> Iterative reconstruction currently supports only voxel sizes of 1 mm or larger, because of restrictions in system memory and computation time.

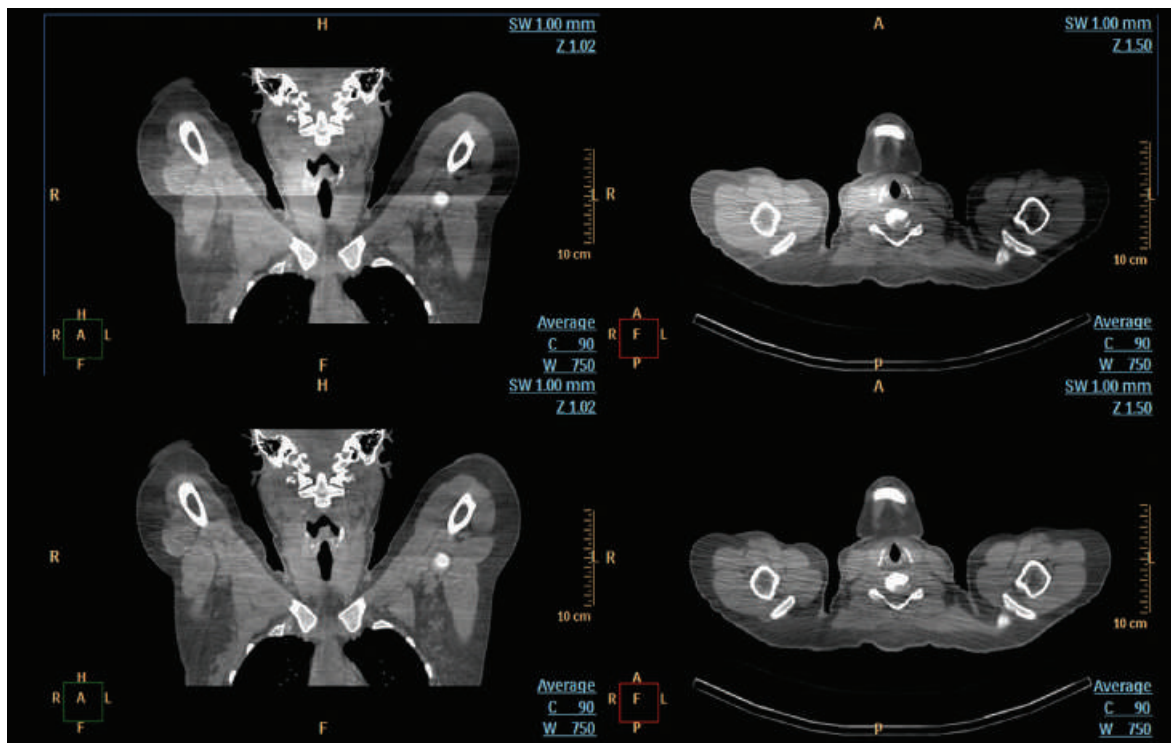
### Patient studies

Figure 6 and Figure 7 show the comparison of the quick review image reconstructed with FBP and the corresponding image obtained with iterative reconstruction for two patient studies. The quick review image provides almost immediate feedback to the user allowing them to quickly evaluate the CT acquisition. As illustrated by Figure 6,

the quick review generally produces good results although some artifacts such as the knit lines between segments can be quite visible. In contrast, the knit lines are much less obvious and the overall uniformity of the image is improved with the iterative reconstruction.



**Figure 6** Quick review image reconstructed with FBP (left) and corresponding image obtained with iterative reconstruction (right). The FBP image provides almost immediate feedback for the CT acquisition while the iterative reconstruction provides improved image quality through better uniformity and reduced noise.



**Figure 7** Quick review image reconstructed with FBP (top) and corresponding image obtained with iterative reconstruction (bottom). In some cases, the approximate nature of the FBP reconstruction algorithm coupled with the offset cone-beam geometry results in HU non-uniformity as can be seen here in the left to right variations in intensity in the FBP image. These intensity variations are significantly reduced with the iterative reconstruction, making the knit line between XCT segments almost disappear.

Figure 7 demonstrates how the approximate nature of the FBP reconstruction algorithm coupled with the offset cone-beam geometry of the XCT system can lead to significant HU non-uniformities causing left to right variations in image intensity. These variations in image intensity tend to accentuate the knit lines. Since the iterative reconstruction algorithm can accurately model the offset cone-beam geometry, these HU

non-uniformities are significantly reduced with the iterative reconstruction, making the knit lines between XCT segments almost disappear.

The low dose localization capabilities of BrightView XCT are illustrated in Figure 8 through Figure 12. These figures show various examples of SPECT/CT localization studies with iterative reconstruction.

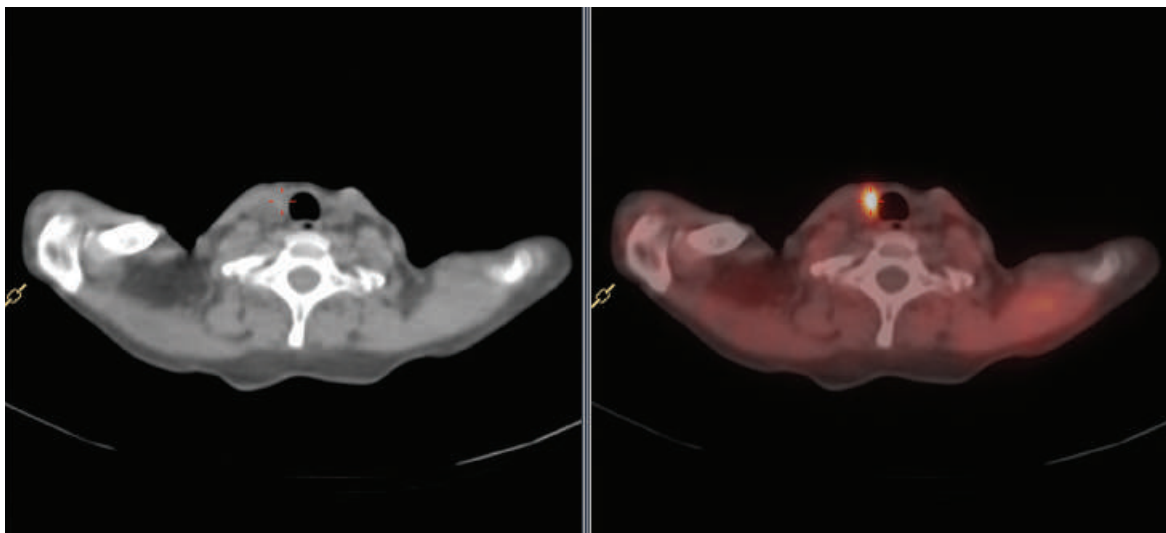


**Figure 8** Transverse views from a SPECT/CT study of a 32 year old female patient with a suspected parathyroid adenoma. Focal uptake of Tc-99m sestamibi identifies the location of the parathyroid adenoma on the XCT image. The effective dose to the patient from the XCT portion of this study was approximately 0.5 mSv.

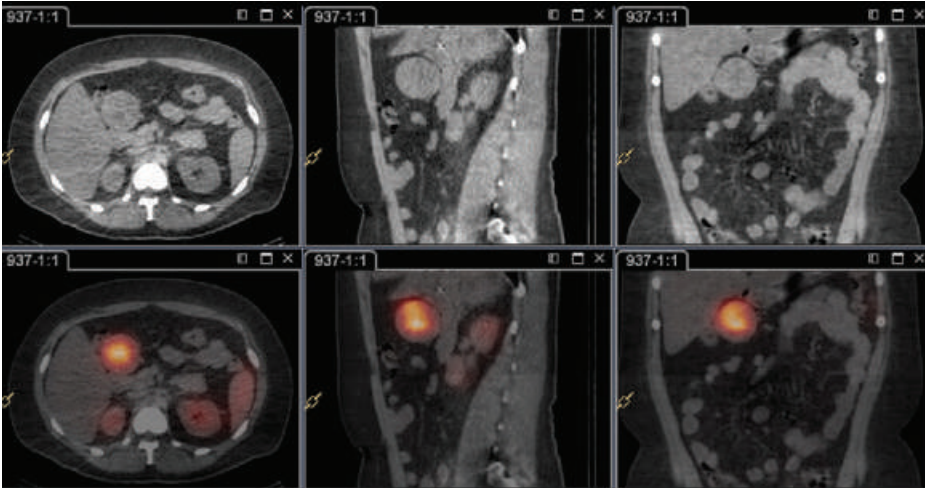


**Figure 9** In-111 Octreotide SPECT/CT study of a patient with a neuroendocrine tumor. Normal physiologic distribution of the radiotracer can be seen in the liver; spleen, kidneys, bowel, and bladder (not visible in the figure). Patient's known mass within the porta hepatis demonstrates marked increased uptake. No additional sites of abnormal uptake to suggest metastatic disease are observed. The effective dose to the patient from the XCT portion of this study was approximately 4.2 mSv.

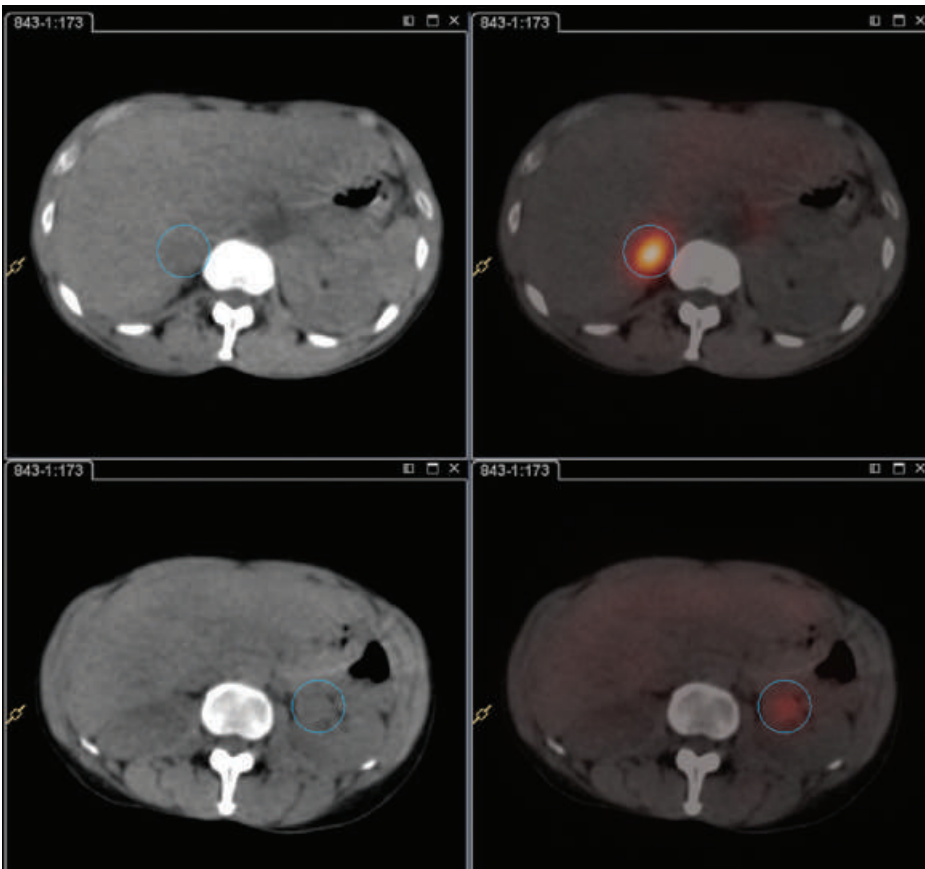


**Figure 10** I-123 MIBG SPECT/CT study of a 54 year old female with an adrenal tumor. Focal uptake in the right adrenal gland (top row) indicates known (biopsy proven) pheochromocytoma. Faint focal uptake in the left adrenal gland (bottom row) suggests second tumor. The effective dose to the patient from the XCT portion of this study was approximately 4.5 mSv.

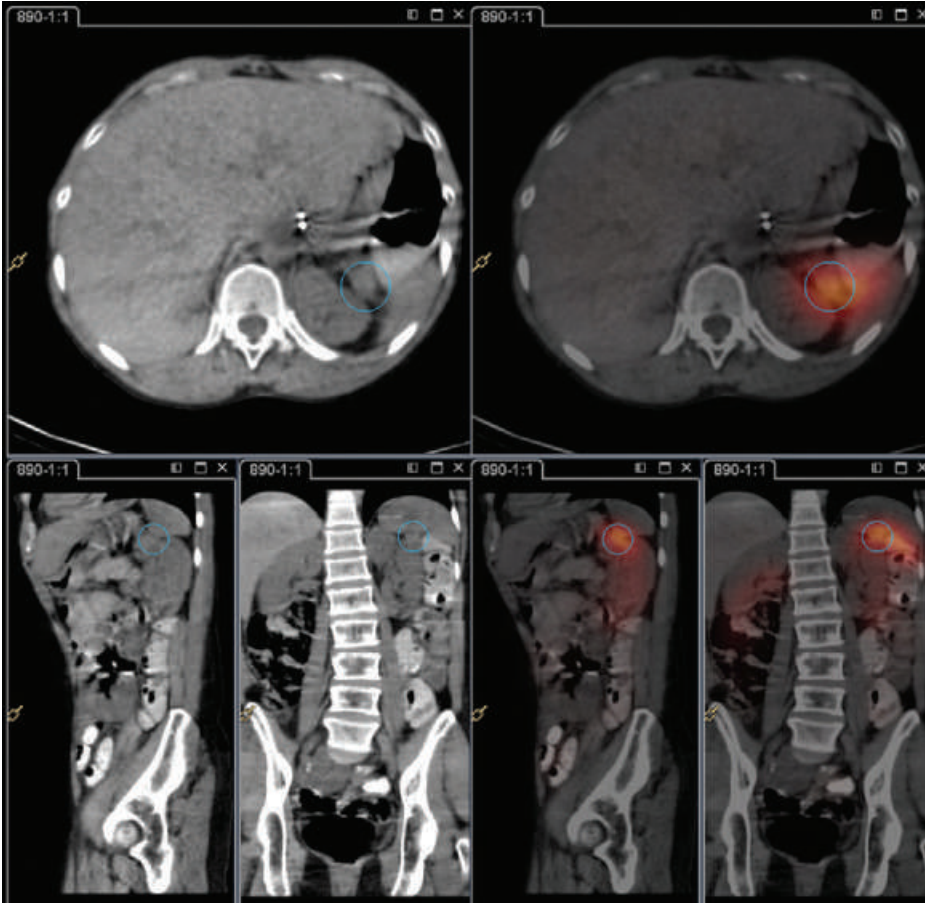


**Figure 11** In-111 Octreotide SPECT/CT images from a patient with epigastric pain and elevated chromogranin A levels. Images showed extensive gastrointestinal bowel activity despite repeated efforts of imaging over one week with high fiber diet and potent bowel laxatives. No definitive persistent foci of increased activity to suggest a carcinoid tumor were observed. The effective dose to the patient from the XCT portion of this study was approximately 4.5 mSv.

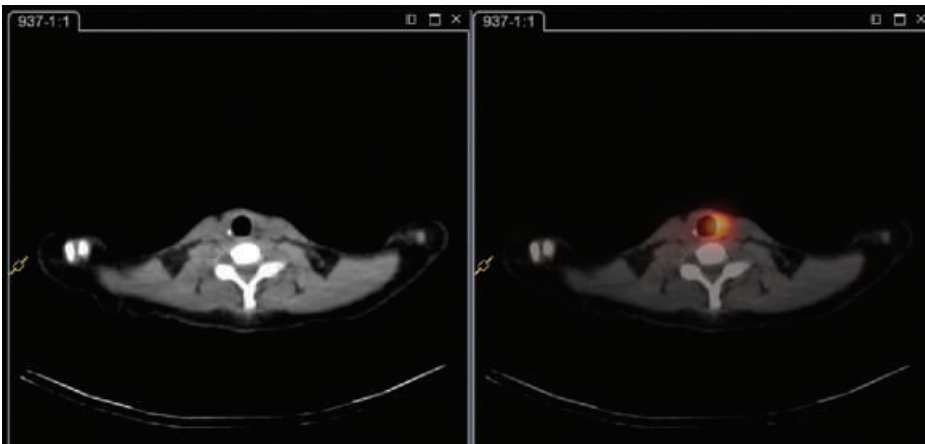


**Figure 12** SPECT/CT images of a 34-year-old female being evaluated for thyroid cancer. Focal uptake of I-123 indicates disease. The effective dose to the patient from the XCT portion of this study was approximately 3.4 mSv.

The high-resolution imaging capabilities of the BrightView XCT are demonstrated in Figure 13 and Figure 14. These figures show high-resolution (0.33 mm voxels) XCT images of the extremities. They were reconstructed with FBP since iterative

reconstruction currently supports only voxel sizes of 1 mm or larger. Nevertheless, as these images reveal, FBP can be used with BrightView XCT to create exquisite high-resolution images of the extremities.

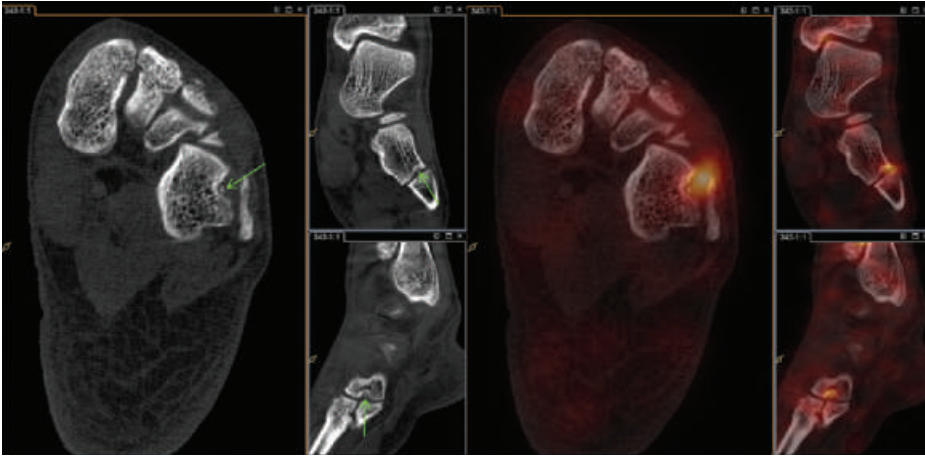


**Figure 13** High resolution (0.33 mm isotropic voxels) XCT image of the foot reconstructed with FBP. The image is of a 41 year old male patient with contusion and distortion of the middle foot with fracture of Os metatarsale IV in 2003 and increasing pain in the outer metatarsus. The XCT image shows a small (1 mm diameter) intra-articular bone fragment (green arrows) in the joint between Os cuboideum and Os metatarsale which corresponds to uptake in the SPECT image. The bone fragment was removed and the patient's medical condition improved. The effective dose to the patient from the XCT portion of this study was approximately 1.5 mSv.

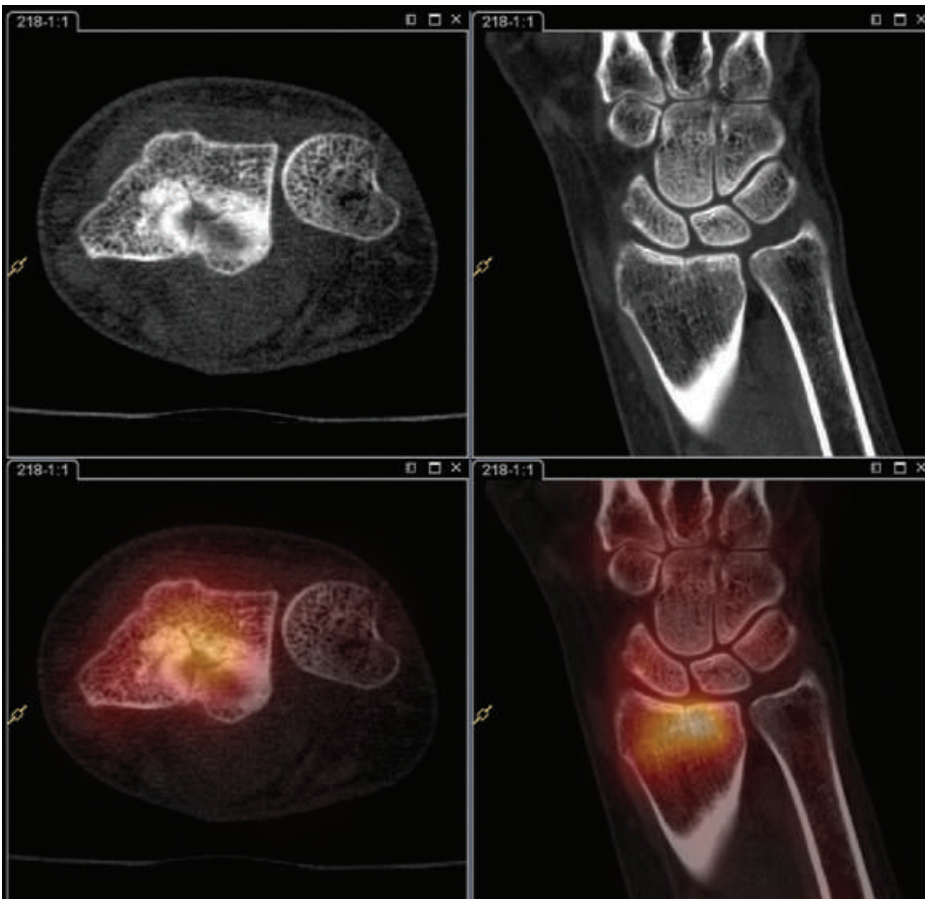


**Figure 14** High resolution (0.33 mm isotropic voxels) XCT image of the wrist reconstructed with FBP. The image is of a 32 year old female patient with chronic right wrist pain after distal radius fracture 5 months earlier. The XCT image shows a star-like residual not yet fused fracture of the distal articular surface of the radius which corresponds to metabolic uptake within the distal radius. The effective dose to the patient from the XCT portion of this study was approximately 1.5 mSv.

In addition to the high resolution XCT studies, FBP is also used for low dose cardiac attenuation scans. Because these scans are acquired over 60 seconds with the patient breathing, there is significant blurring of the data due to motion. These scans are smoothed and down-sampled to match the SPECT voxel size during the generation of the attenuation map. Additionally, the image is segmented prior to converting from HU values to attenuation coefficients. Therefore, the non-uniformities in HU values that can exist with FBP reconstructions do not adversely impact the attenuation map. Furthermore, the iterative reconstruction is more sensitive to motion artifacts than the FBP reconstruction. For these reasons, the iterative reconstruction offers no benefits over FBP for cardiac attenuation scans and only FBP is available for these XCT studies.

### Conclusion

The BrightView XCT with its flat-panel based CBCT component presents a unique SPECT/CT system setup. Because the CBCT component is mounted on the same gantry as the SPECT component, the system has a smaller footprint and system weight compared to SPECT/CT systems that use a separate CT gantry. Furthermore, the flat-panel CBCT component provides low-dose, high-resolution CT images with isotropic voxels. Image reconstruction with FBP and iterative reconstruction are offered to the user. FBP is used to provide a quick volume image for a first review of the acquired data. It is also used for high-resolution (0.33 mm voxel) sub-volume reconstruction of a region of interest and for cardiac attenuation scans. Iterative reconstruction can be used to improve image quality in localization studies.

### Acknowledgements

We would like to thank the following institutions for providing clinical data: Royal Alexandra Hospital, Edmonton, Alberta; Memorial Sloan Kettering Cancer Center, New York, NY; University Hospital Case Medical Center, Cleveland, OH; North Carolina Baptist Hospital, Winston-Salem, NC; Cantonal Hospital Lucerne, Lucerne, Switzerland; and Inselspital Bern, University Hospital, Bern, Switzerland.

### References

1. Sowards-Emmerd D, Balakrishnan K, Wiener J, Shao L, and Ye J. CBCT-subsystem performance of the multi-modality Brightview XCT system. IEEE NSS Conf. Rec. 2009 3053–3058.
2. Hsieh J. Adaptive streak artifact reduction in computed tomography resulting from excessive X-ray photon noise. Med. Phys. 1998 25:2139–2147.
3. Wiegert J, Bertram M, Wiesner S, Thompson R, Brown KM, Morton T, Katchalski I, and Yagil Y. Improved CT image quality using a new fully physical imaging chain. In E. Samei and N. J. Pelc, editors, Medical Imaging 2010: Physics of Medical Imaging, Proc. SPIE 7622:762211.
4. Cho PS, Rudd AD, and Johnson RH. Cone-beam CT from width-truncated projections. Comp. Med. Imag. Graph. 1996 20:49–57.
5. Feldkamp LA, Davis LC, and Kress JW. Practical cone-beam algorithms. J. Opt. Soc. Am. A 1984 1:612–619.
6. Andersen AH and Kak AC. Simultaneous algebraic reconstruction technique (SART): a superior implementation of the ART algorithm. Ultrason. Imag. 1984 25:81–94.
7. Erdoğan H and Fessler JA. Monotonic algorithms for transmission tomography. IEEE Trans. Med. Imag. 1999 18:801–814.
8. Hansis E, Bredno J, Sowards-Emmerd D, and Shao L. Iterative reconstruction for circular cone-beam CT with an offset flat-panel detector. IEEE NSS-MIC 2010 Conf. Rec. Paper M09–231.

**Philips Healthcare is part of  
Royal Philips Electronics**

**How to reach us**

[www.philips.com/healthcare](http://www.philips.com/healthcare)  
[healthcare@philips.com](mailto:healthcare@philips.com)

**Asia**

+49 7031 463 2254

**Europe, Middle East, Africa**

+49 7031 463 2254

**Latin America**

+55 11 2125 0744

**North America**

+1 425 487 7000

800 285 5585 (toll free, US only)

Please visit [www.philips.com/brightviewxct](http://www.philips.com/brightviewxct)



© 2011 Koninklijke Philips Electronics N.V.  
All rights are reserved.

Philips Healthcare reserves the right to make changes in specifications and/or to discontinue any product at any time without notice or obligation and will not be liable for any consequences resulting from the use of this publication.

Printed in The Netherlands.  
4522 962 73251 \* MAY 2011